

Injection of Cooper pairs into quasidiffusive multiwalled carbon nanotubes with weak localization

J. Haruyama,^{1,3,4,*} K. Takazawa,¹ S. Miyadai,¹ A. Takeda,¹ N. Hori,¹ I. Takesue,¹ Y. Kanda,¹ N. Sugiyama,^{2,3} T. Akazaki,⁴ and H. Takayanagi⁴

¹*Aoyama Gakuin University, 6-16-1 Chitosedai, Setagaya, Tokyo 157-8572, Japan*

²*TORAY Research Center, 3-3-7 Sonoyama, Ohtsu, Shiga 520-8567, Japan*

³*JST, CREST, 4-1-8 Hon-machi, Kawaguchi, Saitama 332-0012, Japan*

⁴*NTT Basic Research Laboratories, 3-1 Morinosato-Wakamiya, Atsugi, Kanagawa 243-01, Japan*

(Received 10 June 2003; published 31 October 2003)

We study the influence of Cooper pair injection into niobium (Nb)/quasidiffusive multiwalled carbon nanotube (MWNT's)/aluminum (Al) junctions possessing weak localization. Evaporation of the Nb electrode on the open top end of MWNT's standing in nanopores of alumina membranes makes end-bonded structures possible, leading to highly transparent Nb/MWNT interfaces. We found a proximity-induced conductance increase (PIC), which was enhanced by the extremely large diffusion constant of the Cooper pair in the MWNT's, with onset temperatures as high as $T=6-9$ K. In contrast, we clarified that this PIC was very sensitive to the transparency of the MWNT/Al interface at low temperatures. High transparency led to reentrant conductance due to diffusion out of the Cooper pairs, while we successfully found superconductivity at $T=0.6$ K, implying enhanced critical magnetic fields, in some of the low-transparency samples.

DOI: 10.1103/PhysRevB.68.165420

PACS number(s): 73.23.-b, 73.63.Fg, 74.78.Fk, 74.50.+r

Injection of Cooper pairs into mesoscopic normal (N) conductors [e.g., in superconductor (S)/two-dimensional electron gas (2DEG) junctions and thin metal S/N junction] provides exciting quantum and mesoscopic physics. Cooper pair injection into carbon nanotubes (CN's), a molecular nanoconductor with a variety of quantum phenomena, is also attracting considerable attention. Most of the past investigations have been performed in CN's only in a ballistic electron transport regime.¹⁻⁵ Reference 1 successfully observed proximity-induced superconductivity (PIS), caused by injecting Cooper pairs into ballistic single-walled carbon nanotubes (SWNT's) suspended between the two superconductor electrodes (Re and Ta). They found some anomalous behaviors (e.g., (1) a Josephson current that was not understandable in the framework of Bardeen-Cooper-Schrieffer (BCS) theory, (2) large critical currents, (3) enhanced critical field) in both individual SWNT and SWNT ropes. In particular, the central superconductivity question about Ta/individual-SWNT was how Cooper pairs could coexist with the LL that was yielded by a strong 1D repulsive Coulomb interaction in individual SWNT. This question, which prompted the discussion of the relevance of the presence of superconductivity in a 1D system, is still under debate.^{1,2,6-8} Indeed, Ref. 2 actually reported that a resistance peak which emerged at very low temperature and might originate from multiple Andreev reflections due to the LL in the SWNT, prevented superconductivity in niobium (Nb)/SWNT/Nb junctions.

Recently, it was reported in Ref. 5 that the Kondo effect did not screen Cooper-pair wave functions in aluminum (Al)/ballistic multiwalled carbon nanotube (MWNT)/Al junctions with channel lengths as short as 250 nm when the Kondo temperature is higher than the superconducting gap, implying strong spin entanglement in the MWNT.

In contrast, no one has investigated how Cooper pairs behave in CN's in the diffusive regime. It is well known that MWNT's basically exhibit metallic behavior preserving

phase memory of quantum electron waves in the diffusive regime, which is represented by phase interference phenomena of those waves [e.g., weak localization (WL) and antilocalization (AL), universal conductance fluctuation (UCF), and Altshuler-Aronov-Spivak (AAS) oscillation]. To the best of our knowledge, MWNT's can be ballistic only under certain special conditions (e.g., when electrons flow only in the outermost and second outermost shells) as⁵ mentioned above. In this work we reveal the influence of Cooper pair diffusion through diffusive MWNT's with WL, a constructive phase interference effect of quantum electron waves.

Experimental studies on mesoscopic S /diffusive- N junctions have successfully revealed the presence of a variety of subtle physics only in $S/2$ DEG (Refs. 9-12) and thin metal S/N junctions.¹³⁻¹⁷ When the S/N interface is highly transparent, leakage of the Cooper pair wave function from the S into the N leads to PIS. PIS has also been actively studied in terms of Andreev reflection, in which an incident electron coming from the N is converted into a Cooper pair in the S , leaving a reflected hole in the N at the S/N junction.⁹ In addition, the reentrance effect in the PIS regime has attracted much attention. This effect emerges when the conductance enhancement due to a PIS suddenly decreases at energy levels below the Thouless energy (E_{Th}) that arises from the uncertainty between the diffusion time of the Cooper pair and its energy fluctuation.^{10,13-15} S/N junctions connected to an Aharonov-Bohm (AB) ring also show a variety of attractive mesoscopic phenomena, when magnetic flux was applied into the ring.

Since it is known that quantum electron waves, generated from the molecular band in MWNT's, have the strongest phase coherence among all dirty materials, it is crucial to clarify how Cooper-pair diffusion through MWNT's brings about interesting phenomena. Here, we reveal the existence of a proximity-induced conductance increase, enhanced by a

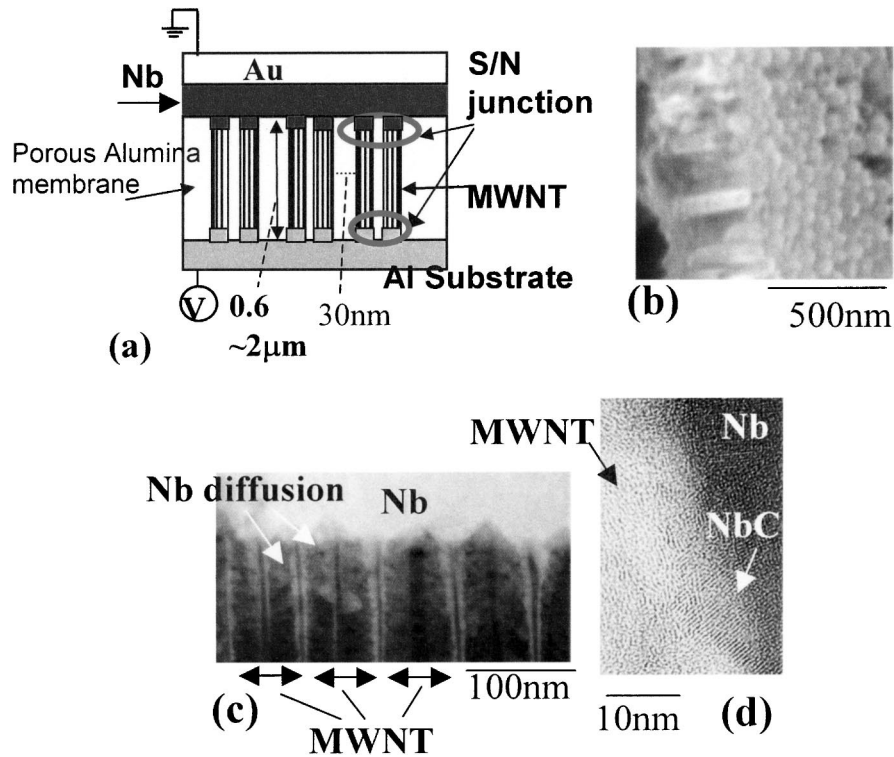


FIG. 1. (a) Schematic cross sections of an array of end-bonded Au/Nb/MWNT/Al junctions, synthesized into the nanopores of alumina membranes by chemical vapor deposition (Refs. 19–21), each with a thickness of $1 \mu\text{m}$ for Au/Nb. T_c of our Nb was about 8.1–9 K and H_c was about 1500 G. The mean outer and inner diameters of the MWNT's are 100 and 60 nm, respectively, with a shell thickness as large as 20 nm. The half-width of the distribution of the outer diameter is less than 15%. The shell structure proving the MWNT has already been reported (Refs. 19 and 20). The measured average characteristics of MWNT's with about $10^3 \sim 10^4$ in one array could exhibit approximately the same properties as those of an individual MWNT (Refs. 19–21), due to the extremely high uniformity. (b) SEM overview image of a MWNT array, standing in the alumina membrane, implying the high regularity and open top portion of MWNT's. (c) High-angle annular dark-field image of a cross sectional TEM (CSTEM) around the Nb/MWNT interface array [see (a)] annealed by the optimal conditions (at 650°C for 30 min), implying a high diffusion of Nb atoms (but at most about 5~10% in volume ratio). No diffusion of Nb into lower ends of MWNT's was also reconfirmed by EDX analyses. (d) High resolution CSTEM image in (b). We use this sample for all the measurements described in this paper. Although bulk NbC is a superconductor with $T_c \sim 11$ K, our NbC should not correspond to this case because it is not bulk and the volume is extremely small.

large diffusion constant, in Nb/quasidiffusive MWNT/Al junctions possessing WL. At low temperatures, we find a reentrant conductance in a highly transparent MWNT/Al interface sample. In contrast, we observe elimination of the reentrant conductance in some low-transparency MWNT/Al interface samples and, then, successfully observe a PIS and Josephson current with enhanced critical magnetic field when this sample was cooled below the T_c of Al.

High transparency of the metal electrode/CN interface is hard to achieve because of the misalignment among chemical potentials, except for the interfaces either including carbide compounds (SiC, TiC) (Ref. 18) or fabricated by a special technique.^{1,3} We successfully realized a highly transparent Nb/MWNT interface by endbonding MWNT's, standing in nanopores of alumina membranes using a Au/Nb (Fig. 1),^{18–21} leading to the presence of NbC at the interface [Fig. 1(d)]. We had already found that slight diffusion of even normal metal electrodes into the top ends of such MWNT's led to a drastic change of phase interference in the bulk of our MWNT's, using this structure.¹⁹ In addition, a highly transparent MWNT/Al-substrate interface was simul-

taneously obtained by this end-bonded structure¹⁹ (but, of course, the resistance of the MWNT/Al interface is higher than that of Nb/MWNT interface, because of the absence of NbC). This is because the annealing temperature is near both the melting point of Al and the synthesis temperature of MWNT. In contrast, in order to make this MWNT/Al interface a lower value, we formed a very thin tunnel barrier with a thickness of only a few nanometers at the bottom end of the MWNT's.²⁰ Annealing this sample led to diffusion of this tunnel barrier into the bottom end of the MWNT (we confirmed this by TEM), resulting in a lower-transparency interface.

First, we report on the conductance behavior in the Nb/MWNT's/Al junction with highly transparent MWNT's/Al interfaces at the other ends. In the inset of Fig. 2(a), the logarithmic magnetic field (H) dependence of normalized zero-bias conductance (G_0) is shown in the sample. This behavior is in good agreement with the calculated result by the formula for two-dimensional weak localization $\Delta G = (e^2/\pi h) \ln[H]$.²⁴ This is consistent with our past work, which reported WL in terms of the logarithmic temperature

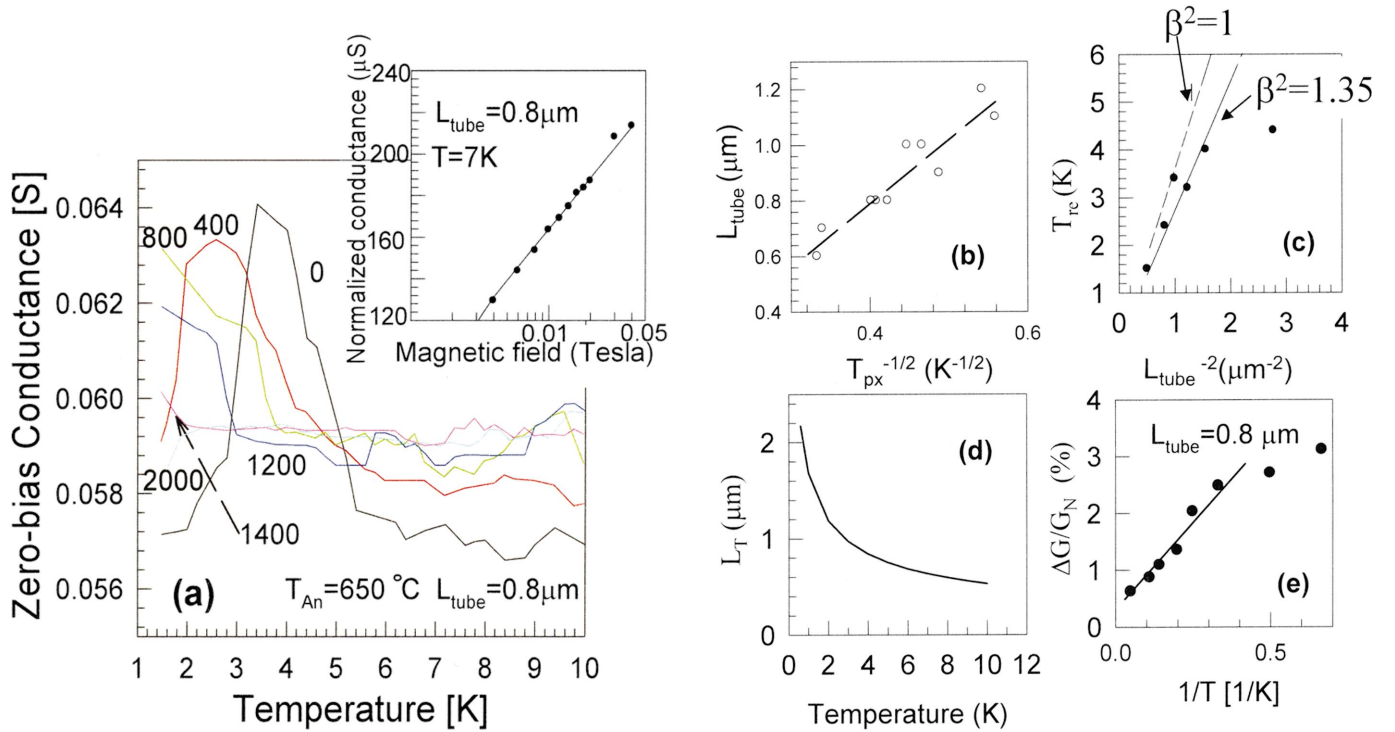


FIG. 2. (Color) (a) Temperature dependences of zero-bias conductance (G_0), in an Nb/MWNT's/Al ($S/N/N'$) junction array with a highly transparent MWNT/Al interface, measured at $T > 1.5$ K for different values of magnetic field perpendicular to the MWNT axis. The labels on the curves correspond to the values of magnetic field in G. The resistance of one MWNT with WL is estimated to be around $100 \text{ K} - 1 \text{ M Ohm}$ at $H = 0$ G, which is consistent with that of MWNT's with WL (Refs. 19, 20). Inset: Normalized G_0 vs logarithmic magnetic field ($\ln[H]$) relationship between $H = 0$ and $H = 400$ G at $T = 7$ K, at which conductance increase does not appear on temperature decrease (see main panel), in the main panel sample. H was applied perpendicular to the MWNT axis. The solid line is the calculated result by the formula for two-dimensional WL (Ref. 24). (b) The L_{tube} vs $T_{px}^{-1/2}$ relationship obtained from measurements of ten samples with the same structure as (a) but with different L_{tube} . The dotted line was obtained using the minimum square method. (c) Transition temperature for the reentrant conductance (T_{re}) vs L_{tube}^{-2} relationship obtained from the six samples in (b). We could not find reentrant conductance in the other four samples in (b). The dotted and solid lines are the results calculated from $T_{Th} = \hbar D/kL^2 = (A/\beta)^2/L^2$ with $L = L_{\text{tube}}$, $A \sim 1.9 \times 10^{-6} \text{ m K}^{1/2}$, and β was a fitting parameter. (d) L_T , estimated from the $D = 0.37 \text{ m}^2/\text{s}$, vs T relationship. (e) Power-law relationship for normalized G_0 magnitude ($\Delta G/G_N$) vs $1/T$ in one of (c) with $T_{re} = 4.5$ K. G_N is the normal state conductance. The solid line is just a guide to the eyes. This result agrees exactly with Ref. 14.

dependence of G_0 and AAS oscillation.^{19,20} This property was observed in all of the samples with an average MWNT length (L_{tube}) greater than $0.8 \mu\text{m}$ and, hence, strongly suggests that, except for the sample with $L_{\text{tube}} = 0.6 \mu\text{m}$, our MWNT's are in the diffusive regime.

In the main panel of Fig. 2(a), we show the temperature dependences of G_0 . We successfully found a gradual but obvious conductance increase with an onset transition temperature (T_{px}) of $T = 5.4$ K under $H = 0$. In contrast, we note that this conductance started to drop from $T = 3.4$ K (i.e., the transition temperature for the conductance decrease $T_{re} = 3.4$ K). T_{px} was shifted to a lower temperature when a magnetic field was applied perpendicular to the tube axis. The critical magnetic field (H_c) for the disappearance of the conductance increase, was about 1400 G, which is mostly the same as H_c of our Nb electrode film. The T_{re} also moved to a lower temperature at $H = 400$ G and then, the conductance drop vanished above $H = 800$ G. The characteristics of the conductance increase and its H dependence are similar to the behavior of superconducting transitions. However, it is remarkable that the conductance does not increase to an infi-

nite value as in general superconducting transitions, due to the conductance drop. Here we found that the " $L_{\text{tube}} = AT_{px}^{-1/2}$ " relationship [Fig. 2(b)], A is a coefficient constant. Importantly, this relationship agrees qualitatively with " $L_T = (\hbar D/kT)^{1/2}$ ", where L_T and D are the thermal diffusion length and the diffusion constant. This agreement stresses that the L_T vs $T^{-1/2}$ relationship becomes dominant in MWNT's below T_{px} . This is straightforward evidence that the conductance increase below T_{px} is strongly associated with the PIS caused by the Nb electrode.

The conductance mechanism follows the smaller of the two parameters; L_T or phase coherence length (L_ϕ). Because L_ϕ in our MWNT's is of the order of a few μm (Ref. 19) at about $T = 10$ K, thereby implying $L_\phi > L_T$ below about $T = 10$ K, we believe that this discussion is relevant. We also reconfirm that such a conductance increase was not observed in any of our MWNT's without superconductor electrodes, despite the fact that we measured over three hundred samples. They just exhibited monotonic conductance decreases due to WL. In these terms, T_{px} can be a critical temperature at which PIS's become dominant compared with

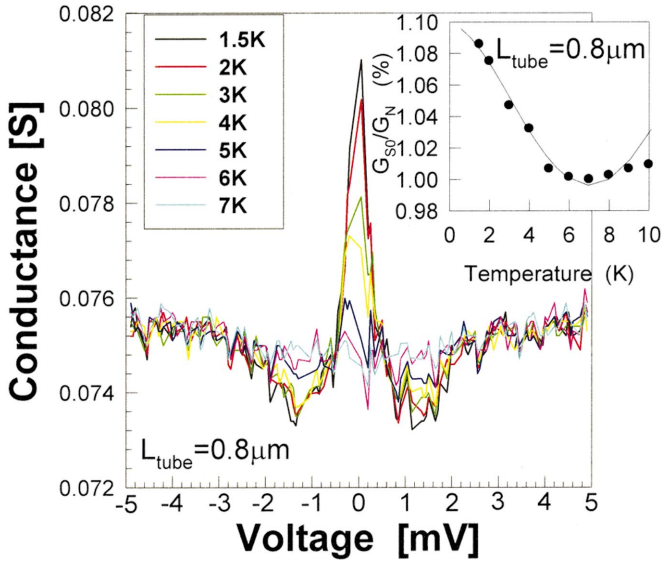


FIG. 3. (Color) Conductance vs voltage relationships on temperature change, around zero bias voltage at $T > 1.5$ K in Nb/MWNT's/Al ($S/N/N'$) junctions with low-transparency MWNT/Al interface. Since the electrode area is twice as big as in the sample for the main panel of Fig. 2(a) owing to the fabrication process, the resistance normalized by area is 1.54 times larger than that in Fig. 2(a). This is consistent with the low-transparency MWNT/Al interface. Inset: A monotonic increase of normalized G_0 on temperature decrease, corresponding to the main panel, without the reentrance effect. The solid line is the calculated result using the equation proposed in Ref. 9.

a conductance decrease due to WL as the temperature decreases. In general PIS can even occur at the N -channel length $\gg L_T$, leading to shrinkage of the N length (e.g., by Maki-Thompson-Larkin fluctuations of the order parameters).^{10,14} From this viewpoint, it is shown in the latter part of this paper that conductance enhancement by PIS starts to appear when L_T attains about 75–85 % of each L_{tube} , as the temperature lowers [Fig. 2(d)].

Here, we argue that the conductance drop at $T_{re} = 3.4$ K in Fig. 2(a) is due to the reentrance effect, which is critical for manifestation of the PIS regime. The N -channel/ N -reservoir (N/N') junction attached to the other end of the N channel, plays an important role in this context (i.e., MWNT/Al-substrate junction in our system). When the N/N' interface is highly transparent, the proximity-induced Cooper pair amplitude is suppressed near the N/N' junction because the Cooper pairs diffuse out of the N channel through the interface. In the N channel edge around this N/N' interface, electrons feel the $E_{\text{Th}} (= \hbar D/L^2)$ gap rather than Δ , where Δ and L are the bulk superconducting gap and the N channel length, respectively, because the diffusion becomes a dominant phenomenon. This leads to the spatially averaged normalized density of state $[N_N(E)]$ in the N channel being less than its normal state value, at $E \leq E_{\text{Th}}$. Consequently, the conductance decreases at $E \leq E_{\text{Th}}$ (i.e., the reentrance effect), whereas the PIS can survive only at $E \geq E_{\text{Th}}$.

Toyoda *et al.*¹⁰ created the reentrance effect by controlling D and, hence, $E_{\text{Th}} (= \hbar D/L^2)$, by systematically chang-

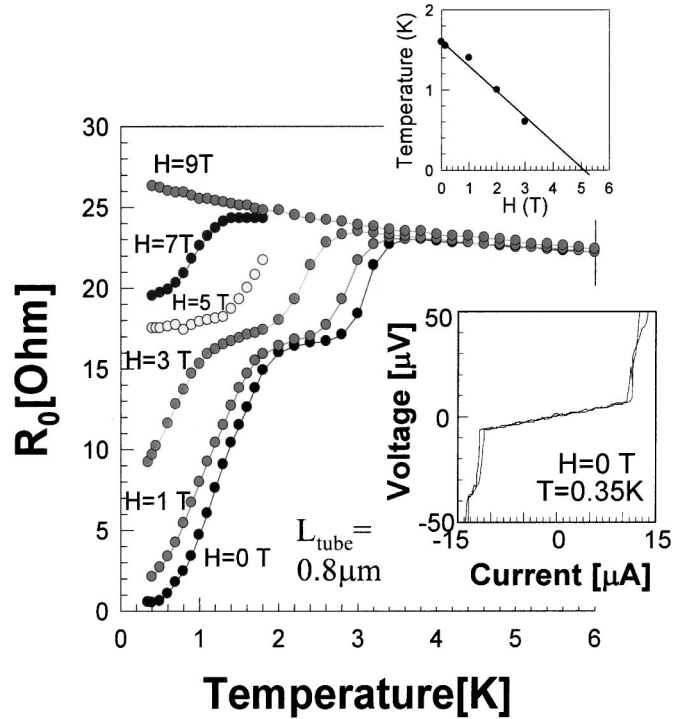


FIG. 4. Temperature dependences of zero-bias resistance (R_0), which were cooled below $T = 1.2$ K, in Fig. 3, for different values of magnetic field perpendicular to the MWNT axis. The labels on the curves correspond to T_e . Because a quasi-four-terminal method was applied for each measurement, this main panel and the lower inset include the contact resistance (less than 1Ω) for the lead lines. Lower inset: Proximity-induced Josephson supercurrent. Upper inset: Field dependence of the transition temperature, which was defined as the inflexion point of $R_0(T)$.

ing the carrier density (N_s) in the N by the gate voltage in the Nb/2DEG junction. Instead of this, we identify a reentrance effect by changing the length of the N channel (i.e., L_{tube}). In Fig. 2 (c), we show the T_{re} vs L_{tube}^{-2} relationship obtained from the measurement results of the samples used for Fig. 2(b). Interestingly, this relationship is mostly linear except at $L_{\text{tube}} = 0.6 \mu\text{m}$. This result agrees qualitatively with the Thouless temperature (T_{Th}) dependence on the N -channel length L (i.e., $T_{\text{Th}} = \hbar D/kL^2$). As explained above, because the $L_{\text{tube}} = AT_{px}^{-1/2}$ relationship in Fig. 2(b) ($A = 1.9 \times 10^{-6} \text{ m K}^{1/2}$) was qualitatively equivalent to $L_T = (\hbar D/kT)^{1/2}$, we define $A = \beta(\hbar D/k)^{1/2}$, where β is a constant coefficient. With $T_{\text{Th}} = \hbar D/kL^2 = (A/\beta)^2/L^2$, we can derive the T_{Th} vs L_{tube}^{-2} relationship, by using $A \sim 1.9 \times 10^{-6} \text{ m K}^{1/2}$, $L = L_{\text{tube}}$, and β as a fitting parameter. From the data shown in Fig. 2(b), the value $\beta^2 = 1.35$ gives the best fit to the measurements in the linear section. This $\beta^2 = 1.35$ value establishes the relationship $T_{re} = 0.74 \times T_{\text{Th}}$ which agrees quantitatively with those observed in the reentrance effect in the Nb/2DEG junction ($T_{re} = 0.4 \times T_{\text{Th}}$) (Ref. 10) and in the Al/Cu junction ($T_{re} = 0.5 \times T_{\text{Th}}$) (Ref. 14).

The highest $T_{re} = 4$ K in Fig. 2(c), except for that at $L_{\text{tube}} = 0.6 \mu\text{m}$, is much higher than that reported in Nb/2DEG ($T_{re} = 0.5$ K) (Ref. 10) and in the Al/Cu junctions

($T_{re} = 60$ mK) (Ref. 14). This is a manifestation of the extremely high diffusivity $D = 0.37$ m²/s, estimated from the parameters $A \sim 1.9 \times 10^{-6}$ m k^{1/2} and $\beta^2 = 1.35$, in our MWNT's (e.g., $D = 0.08$ m²/s at most, in the case of 2DEG and $D = 0.007$ m²/s in the Cu film), resulting in strong phase coherence. This $D = 0.37$ m²/s is also four times larger than that of past reports in MWNT's.²² The appropriateness of $D = 0.37$ m²/s is also proven for the data in Figs. 3 and 4 shown later. From this discussion, we conclude that the reentrance effect can occur even in a diffusive MWNT. This conclusion is consistent with a highly transparent MWNT/Al-substrate (N/N') interface. The high carrier density, which was introduced by the efficient injection of Cooper pairs through the highly transparent Nb/MWNT interface, could be the origin for this large D .

Figure 2(d) shows L_T , estimated from $D = 0.37$ m²/s, at each temperature. Comparison of Fig. 2(d) with Fig. 2(b) indicates that conductance enhancement by PIS starts to emerge when the Cooper pair wave function (i.e., L_T) diffuses to positions of about 75–85% from the Nb/MWNT interface in each L_{tube} , as temperature lowers, when we neglect the influence of WL.

Here, a mean free path (l_e) is estimated to be as long as 0.74 μ m, when one simply uses the relationship $D = V_F l_e / 2$ and $V_F = 10^6$ m/s, which is the Fermi velocity in MWNT.²² Because this means $L_{tube} = 0.6$ μ m $< l_e = 0.74$ μ m, the MWNT with $L_{tube} = 0.6$ μ m is in the ballistic regime and, hence, discussion in the diffusion regime here cannot apply to this sample. This is consistent with the departure of T_{re} from the linear regime in the MWNT with $L_{tube} = 0.6$ μ m [Fig. 2(c)] (i.e., a weakening of the reentrance effect in the ballistic regime). In addition, this is also consistent with the absence of the WL property as shown in the inset of Fig. 2(a), in the $L_{tube} = 0.6$ μ m sample. In this sense, our MWNT's with the $L_{tube} \geq 0.8$ μ m can be in the quasidiffusive regime, strictly speaking. However, the study of Cooper-pair diffusion in 2DEG has been successfully performed even in such a regime.¹⁰

The temperature dependence of the normalized G_0 [Fig. 2(e)] also supports the presence of the reentrance effect. Charlat *et al.*¹⁴ showed that the power-law decay of $\Delta G/G_N$ on temperature increases with the ratio being between 2.5 and 0.5% and its saturation below $T_{re} (= 50$ mK). These are quantitatively in precise agreement with Fig. 2(e).

Next, we show the normalized conductance (G_{S0}/G_N) property at $T > 1.5$ K in Nb/MWNT's/Al junctions with a low-transparency MWNT/Al interface on the other end (the inset of Fig. 3). Interestingly, in some samples of this type, only the monotonic G_{S0}/G_N increase is observable from $T = 6$ K down to $T = 1.5$ K as the temperature decreases. Because this $T = 6$ K approximately corresponds to the T_{px} of MWNT's with $L_{tube} = 0.8$ μ m [see Fig. 2(b)], this conductance increase can be due to PIS's. As explained above, because this low-transparency MWNT/Al interface suppresses diffusion out of the Cooper pairs to the Al substrate, the reentrance effect disappears. This strongly supports the claim for the reentrance effect mentioned above.

The main panel of Fig. 3 also shows the G_0 vs voltage relationship around Δ of Nb on temperature decrease. A conductance peak around zero voltage monotonically grows with $\Delta = 1.3$ meV ($\approx \Delta_{Nb} \sim 1.4$ meV) from $T = 6$ K ($\approx T_{px} = 6$ K) with decreasing temperature, whereas two conductance dips monotonically deepen between the voltage regions of $\pm 0.6 - \pm 2$ mV also at $T = 6$ K. The very sharp conductance valley observable at a voltage of $+0.2$ mV disappears as the temperature decreases. It is already known that Andreev reflection with a highly transparent S/N interface leads to the growth of a conductance peak.^{2,6,9,23} The characteristics of the increasing G_0 peak are qualitatively similar to those in Refs. 6, 9, and 23. In particular, Kastalski *et al.*⁹ showed that the Nb/InGaAs junction exhibited exactly the same properties as ours. Therefore, this growth in the conductance peak is also evidence for the highly transparent Nb/MWNT interface without the reentrance effect and the consequent PIS. Here, we try to reconfirm whether the conductance increase shown in the inset of Fig. 3 is due to PIS's, using the equation $G_{S0}/G_N = TL_T \tau_\Delta \ln^2(T_c/T)$, where τ_Δ is the order parameter relaxation time.⁹ Based on the *ad hoc* assumption that $\tau_\Delta \propto T^{-\alpha}$ with $\alpha \ll 1$, G_{S0}/G_N varies as $T^{-\alpha+1} L_T \ln^2(T_c/T)$. In fact, the data and calculation result are in good agreement (inset of Fig. 3). The best fit using $D = 0.37$ for L_T gives $G_{S0} = 0.1 G_N T^{3.5} L_T \ln^2(T_c/T)$, resulting in $G_N = 0.0747 S$ and $\alpha = -2.5$. Therefore, we conclude that the conductance increase in Fig. 3 can be attributed to Andreev reflection and PIS.

When this was cooled below $T = 1.2$ K, we could successfully find a superconducting transition, due to PIS and $S/N/S$ structure, at $T_c = 0.6$ K (main panel of Fig. 4) and clear proximity-induced supercurrent (lower inset of Fig. 4). These behaviors are very similar to ballistic SWNT systems¹ at least for the following two terms. (1) The resistance drop at zero-magnetic field is gradual on temperature decrease, with two steps between the onset temperature and T_c (main panel). (2) The transition between the superconducting state and the dissipative state is very abrupt, showing hysteresis loops above I_c (lower inset).

The first term will be interpreted by as a pinning of spreading out of Cooper pair wave function (i.e., increase of L_T) due to defects or impurities in the MWNT's when temperatures lowered. This is consistent with the low-transparent Al/MWNT interfaces, which were formed in order to suppress the reentrant effect and with the quasidiffusive carrier transport in our MWNT's. The second term was also discussed from the viewpoint of the phase-slip center, in which the normal state appears around defects above I_c .¹ This may be consistent with the explanation for the first term, because defects play an important role in both phenomena. It is interesting that these similarities are observed in both the ballistic and diffusive CN's. This may indicate a large sensitivity of the Cooper-pair wave function in CN's to defects or impurities.

However, as the most striking difference from the case in SWNT's, we found that the R_0 vs temperature relationship in the main panel of Fig. 4 mostly does not change when $H = 1$ T was applied and that the $H_c = 5.2$ T estimated from the upper inset of Fig. 4 was surprisingly about 35 times larger

than $H_c = 0.15$ T of our Nb electrode. In addition, this ratio is about four times larger than the ratio of H_c 's between the SWNT and the Ta electrode connected to it (10 times).¹ This result may be associated with the possibility that our MWNT can maintain strong spin coherence and its entanglement in spin singularity for the applied magnetic field. In fact Ref. 5 experimentally turned out strong spin entanglement in the ballistic MWNT by successful observation of the coexistence of a Kondo singlet and PIS.

The reason for this high H_c is not yet clear. Even the third H_c (H_{c3}) of Nb (i.e., presence of surface superconductivity) cannot explain this, because the thickness of Nb electrode is $1 \mu\text{m}$ ($>$ phase coherence length) and only $H_{c3} \sim 1.695H_{c2}$ (0.15 T). The inverse proximity effect, in which the T_c of the Pb film and its Δ were enhanced with slightly increasing Ag thickness in 2D ultrathin superconducting quench-condensed Pb film with an overlayer of Ag,¹⁷ cannot explain such a 35-times larger H_c . Because the addition of quasiparticles from the Ag layer suppressed the strong Coulomb interaction, which degraded T_c and Δ , in the Pb film and enhanced the electron screening in the system, the inverse proximity effect took place. Our Nb film is not similar to the case of this Pb film. Therefore, more careful investigation is required to reveal the origin of this anomaly.

In addition to the results presented here, more investigation will be required to fully understand PIS's in diffusive

MWNT's. Why some samples have the reentrant conductance and the others have supercurrents is not yet perfectly understood and controlled, even in terms of the MWNT's/Al interfaces presented here. The appearance of supercurrents in the low-transparency MWNT's/Al interface samples also seems to be not consistent with general supercurrents through $S/N/S$ junctions here. Anyway, it is sure that this is very sensitive to the interface transparency of MWNT's/Al junctions. However, our method utilizing nanoporous alumina membranes can be a powerful tool to easily realize end-bonded CN's and the highly transparent interface of metal/CN junctions. If there exist the strong spin-phase coherence and spin entanglement without strong electron interaction unlike SWNT's, MWNT's must be a molecule favorable to quantum computation and teleportation.

We sincerely thank H. Bouchiat, H. Shinohara, B. Altshuler, C.M. Marcus, R. Mohanty, M.S. Dresselhaus, Ph. Avouris, D. Tomanek, L. Kouwenhoven, and J.-P. Leburton for fruitful comments, discussions, and encouragement. This work was supported by Carbon Nanotube Electronics from the Special Coordination Funds for Promoting Science and Technology of the Ministry of Education, Culture, Sports, Science and Technology of the Japanese Government, and by the fund of Promotion of Material and Science Technology (MST).

*Email address: j-haru@ee.aoyama.ac.jp

¹A. Yu. Kasumov *et al.*, *Science* **284**, 1508 (1999).

²F. Morpurgo, J. Kong, C. Marcus, and H. Dai, *Science* **286**, 263 (1999).

³M. Kociak *et al.*, *Phys. Rev. Lett.* **86**, 2416 (2001).

⁴Z. K. Tang *et al.*, *Science* **292**, 2462 (2001).

⁵M. R. Buitelaar, T. Nussbaumer, and C. Shonenberger, *Phys. Rev. Lett.* **89**, 256801 (2002).

⁶Y. Wei *et al.*, *Phys. Rev. B* **63**, 195412 (2001).

⁷D. L. Maslov *et al.*, *Phys. Rev. B* **53**, 1548 (1996); R. Fazio, F. W. J. Hekking, and A. A. Odintsov, *ibid.* **53**, 6653 (1996).

⁸D. Loss and T. Martin, *Phys. Rev. B* **50**, 12 160 (1994); P. Recher and D. Loss *ibid.*, **65**, 165327 (2002).

⁹A. Kastalsky *et al.*, *Phys. Rev. Lett.* **67**, 3026 (1991).

¹⁰E. Toyoda, H. Takayanagi, and H. Nakono, *Phys. Rev. B* **59**, R11 653 (1999).

¹¹H. Takayanagi, J. Bindslev Hansen, and J. Nitta, *Phys. Rev. Lett.* **74**, 162 (1995); **74**, 166 (1995).

¹²H. Fukuyama *et al.*, *J. Phys. Soc. Jpn.* **55**, 1814 (1986).

¹³S. G. den Hartog *et al.*, *Phys. Rev. B* **56**, 13 738 (1997).

¹⁴P. Charlat *et al.*, *Phys. Rev. Lett.* **77**, 4950 (1996).

¹⁵A. A. Golubov, F. K. Wilhelm, and A. D. Zaikin, *Phys. Rev. B* **55**, 1123 (1997).

¹⁶V. T. Petrashov, V. N. Antonov, P. Delsing, and R. Claeson, *Phys. Rev. Lett.* **70**, 347 (1993).

¹⁷O. Bourgeois, A. Frydman, and C. Dynes, *Phys. Rev. Lett.* **88**, 186403 (2002).

¹⁸R. Martel *et al.*, *Phys. Rev. Lett.* **87**, 256805 (2001); Y. Zhang *et al.*, *Science* **285**, 1719 (1999).

¹⁹J. Haruyama, I. Takesue, and T. Hasegawa, *Phys. Rev. B* **65**, 033402 (2002); *Appl. Phys. Lett.* **79**, 269 (2001); **81**, 3031 (2002).

²⁰J. Haruyama, I. Takesue, T. Hasegawa, and Y. Sato, *Phys. Rev. B* **63**, 073406 (2001); *Appl. Phys. Lett.* **77**, 2891 (2000).

²¹C. Papadopoulos, A. Rakitin, J. Li, A. S. Vedenev, and J. M. Xu, *Phys. Rev. Lett.* **85**, 3476 (2000).

²²L. Forro and C. Schonenberger, in *Carbon Nanotubes*, edited by M. Dresselhaus, G. Dresselhaus, and P. Avouris (Springer, Berlin, 1996), pp. 340, 358, 359.

²³G. E. Blonder, M. Tinkham, and T. M. Klapwijk, *Phys. Rev. B* **25**, 4515 (1982).

²⁴S. Kobayashi, *Surf. Sci. Rep.* **16**, (1992).